In-situ synthesis of self-standing SbBi-porous carbon fibers enabling ultra-stable sodium-ion storage

Zheng Li[a#], Hanghang Liu[a#], Jiale Cao[a], Xueying Zhang[a], Qing Zhu[a], Ying Yin[c], Jinliang Li*[b] and Botian Liu*[a]*

[a]Guangxi Key Laboratory of Electrochemical and Magneto-chemical Functional Materials, Guilin University of Technology, Guilin 541004, China

[b]Siyuan Laboratory, Guangdong Provincial Engineering Technology Research Center of Vacuum Coating Technologies and New Materials, Guangdong Provincial Key Laboratory of Nanophotonic Manipulation, Department of Physics, College of Physics & Optoelectronic Engineering, Jinan University, Guangzhou 510632, China

[c]Shenzhen Automotive Research Institute, Beijing Institute of Technology, Shenzhen 518118, Guangdong, China

[#] Contributed equally to this work

*Corresponding author:

Email: yinyingupc@gmail.com (Y. Yin); lijinliang@email.jnu.edu.cn (J. Li); btliu2018@glut.edu.cn (B. Liu).

1. Experimental section

Synthesis of the SbBi-PCF anode

The SbBi-PCF anode was prepared using a combined electrospinning and annealing process. Typically, 0.5 g of $Bi(NO_3)_3{\cdot}5H_2O$, 0.23 g of $SbCl_3$, 0.2 g of $Zn(CH_3COO)_2{\cdot}2H_2O$, and 1.2 g of PAN were dissolved in 10 mL of DMF and stirred using a magnetic stirrer at room temperature for 24 h. The resulting solution was then transferred into a 10 mL plastic syringe with a stainless steel nozzle and subsequently placed into a commercial electrospinning machine. In the electrospinning process, a high voltage of 20 kV was applied with a flow rate of 0.4 mL h^{-1} through the needle positioned 15 cm away from the Al foil wrapped around a metal drum rotating at 10 rpm. The as-prepared films were first stabilized at 250 °C for 2 h in air and then transferred to a tube furnace, which was carbonized in a nitrogen atmosphere at 700 °C for 3 h with a heating rate of 2.5 °C min^{-1} to produce SbBi-PCF films. For comparison, the CF films were prepared by a similar procedure without adding Bi, Zn, and Sb sources.

Synthesis of the NVP/CF cathode

The NVP/CF cathode was prepared using a combined electrospinning and annealing process. Typically, 0.24 g of NaH_2PO_4, 0.155 g of NH_4VO_3, 0.168 g of $C_2H_2O_4{\cdot}2H_2O$, and 1.2 g of PAN were dissolved sequentially in 10 mL of DMF and stirred using a magnetic stirrer at room temperature for 24 h. And then, the homogeneous blue solution was transferred into a 10 mL plastic syringe with a stainless steel nozzle and subsequently placed into a commercial electrospinning machine. In the electrospinning process, a high voltage of 25 kV was applied with a flow rate of 0.5 mL h^{-1} through the needle positioned at 15 cm away from the Al foil wrapped around a metal drum rotating at a speed of 10 rpm. Subsequently, the as-prepared films were first stabilized at 250 °C for 2 h in air and then transferred to a tube furnace carbonized in a nitrogen atmosphere at 800 °C for 2 h with a heating rate of 2.5 °C min^{-1} to produce a self-standing NVP/CF cathode.

Electrochemical measurement

All electrochemical measurements were carried out in a two-electrode

configuration, where a glass microfiber filter (Whatman, GF/B) served as the separator and a 1 M $NaClO_4$ solution was dissolved in a mixture of propylene carbonate and fluoroethylene carbonate (5 wt%) as the electrolyte. The free-standing NVP/CF films were cut into squares with a side length of 10 mm, serving as the work electrode; each square presented an average loading of 0.5 mg cm^{-2}. The self-standing SbBi-PCF films were cut into squares with a side length of 10 mm, serving as the work electrode; each square had an average loading of 0.7 mg cm^{-2}. To evaluate the Na-ion storage performance of the electrode, CR2032 coin cells were assembled in a glovebox (Etelux, Lab2000) under Ar with O_2 and H_2O contents of less than 0.1 ppm. For the SbBi-PCF anode, the battery test system (Neware BTS4000) was employed to record the GCD profiles and GITT data, with a voltage range of 0.01-3 V and a current density of 100 mA g^{-1}. CV tests were conducted using an electrochemical workstation (Shanghai Chenhua) at a scan rate of 0.2 mV s^{-1} within the voltage range of 0.01 to 3 V. For the NVP/CF cathode, the battery test system (Neware BTS4000) was used to record GCD profiles and CV curves, with a voltage range of 4-2 V and a current density of 100 mA g^{-1}. EIS are obtained by applying a sine wave with amplitude of 5.0 mV over the frequency range from 100 kHz to 0.1 Hz. The specific capacity of anode or cathode was calculated based on their total mass in the manuscripts. For the full cell, the battery test system (Neware BTS4000) was used to record GCD profiles and CV curves, with a voltage range of 1-4.2 V. The specific capacity and energy/power density of the full cell were calculated based on the total mass of the cathode in the manuscript.

Materials characterizations

The samples were characterized using a scanning electron microscope (Zeiss, 5.0~20.0 kV) with an EDS detector, XPS (Thermo Electron, VG ESCALAB 250 spectrometers using Al Kα radiation), XRD (Bruker, D8 Avance diffractometer with a Cu-Kα radiation source), and a transmission electron microscope (JEOL, JEM-2100F, 200 keV). The detailed information about pores was measured using the Brunauer-Emmett-Teller (BET) equation based on the nitrogen adsorption/desorption isotherm obtained using a surface analyser (Quantachrome version 3.0).

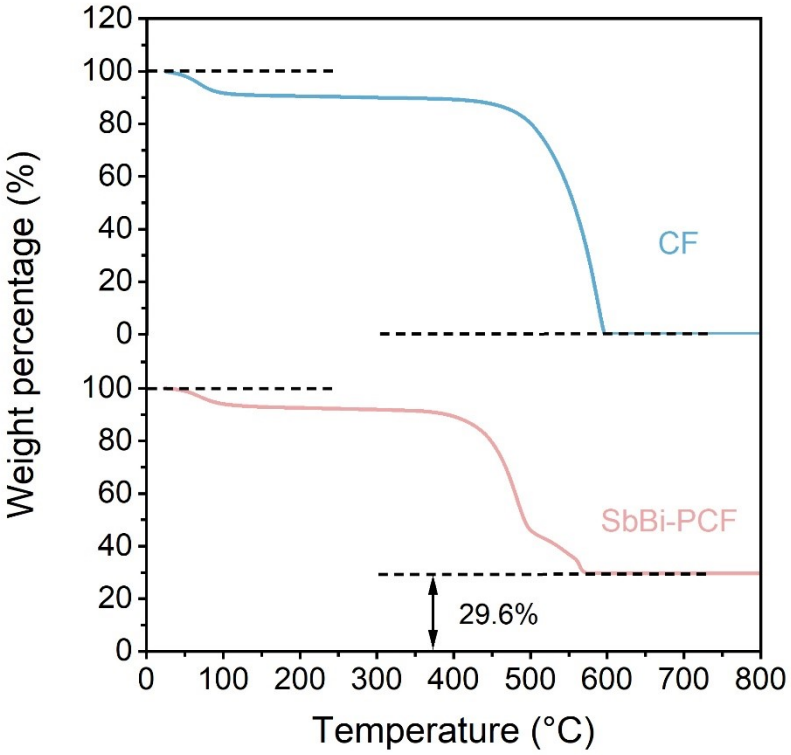

Fig. S1 TGA curves of CF and SbBi-PCF sample

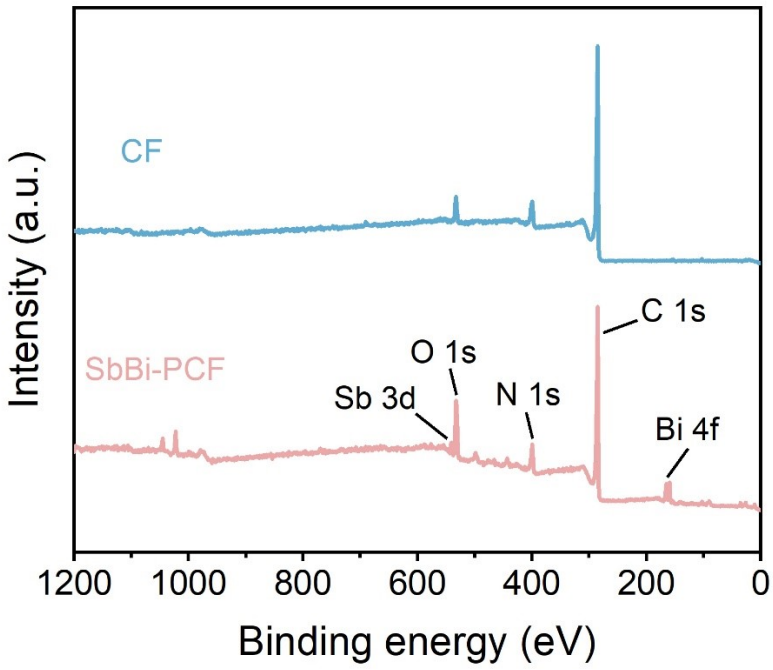

Fig. S2 XPS full spectrum of CF and SbBi-PCF.

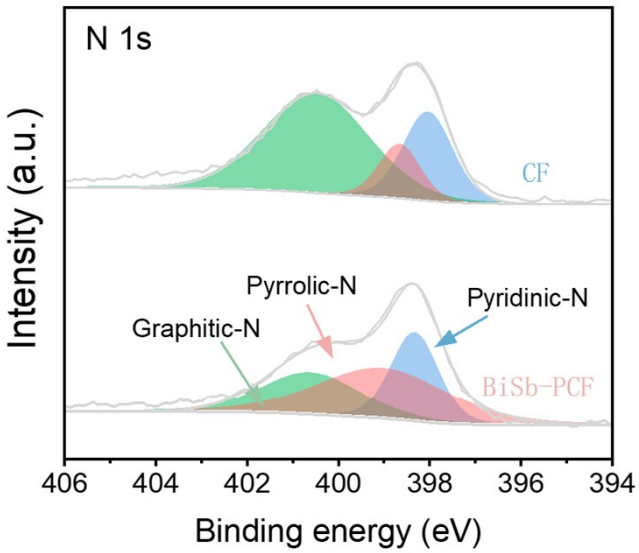

Fig. S3 High-resolution XPS spectra of N 1s for CF and SbBi-PCF

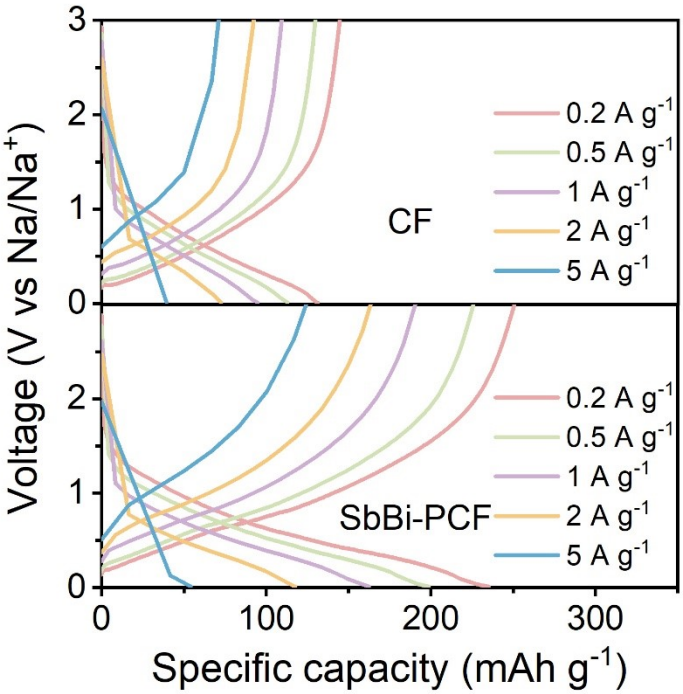

Fig. S4 GCD curves of CF and SbBi-PCF anode at various current densities

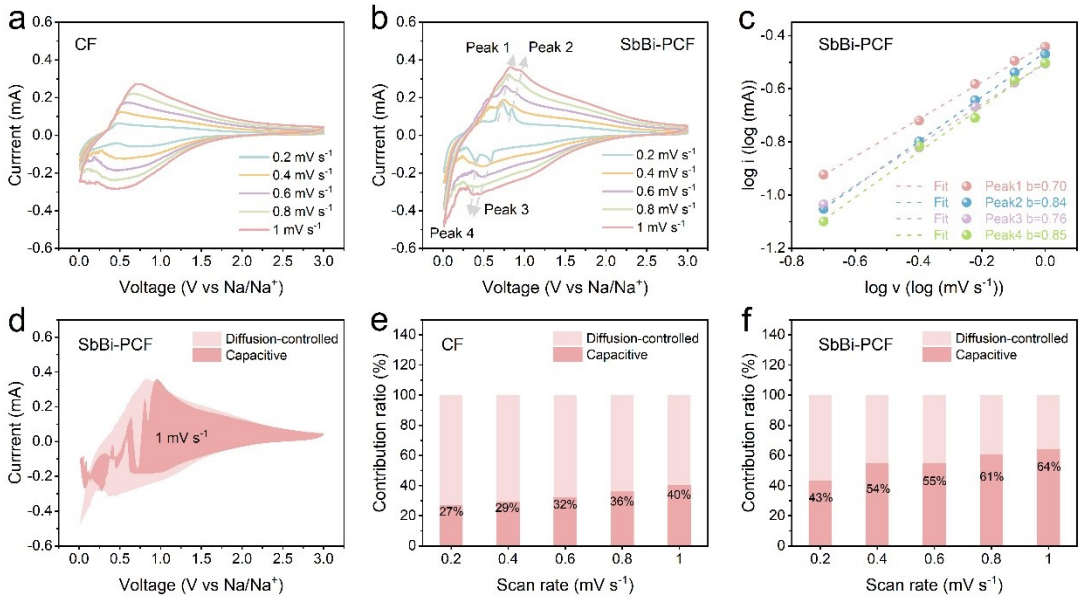

Fig. S5 CV curves of (a) CF and (b)SbBi-PCF at different scan rates; (c) relationship between log (i) and log (v) of SbBi-PCF; (d) capacitive contribution area of SbBi-PCF at 1 mV s^{-1}; capacitive contribution ratios of (e) CF and (f) SbBi-PCF at different scan rates.

All CV curves show similar shape except some peak shifts. These peak shifts are attributed to the contribution of capacitive behavior, and the relationship are calculated between peak current (i) and scan rate (v) as follows:

$$i = av^b \qquad \text{(S1)}$$

It is obtained the following equation by transformation:

$$\log i = b\log v + \log a \qquad \text{(S2)}$$

Where a and b are adjustable parameters. Both of them, the value of b determines the sodium storage process. According to the behavior of the battery, ion diffusion dominates the sodium storage reaction of the electrode when the b value is close to 0.5, and the capacitive behavior maintains dominance when the b value is close to 1. In addition, the contribution of capacitive is quantified by the following Equation:

$$i(V) = k_1 v^{\frac{1}{2}} + k_2 v \qquad \text{(S3)}$$

where k_1, k_2 are the equation parameters, and i(V) is the current response. $k_1 v^{1/2}$ is on behalf of the quantity of diffusion-controlled behavior and $k_2 v$ represents the fraction of capacitive behavior. The above equation is transformed into:

$$i(V)/v^{\frac{1}{2}} = k_1 x + k_2 v^{\frac{1}{2}} \qquad \text{(S4)}$$

After transformation, k_1 and k_2 are calculated by the $i(V)/v^{1/2}$ versus $v^{1/2}$, and the capacitive current can be obtained.

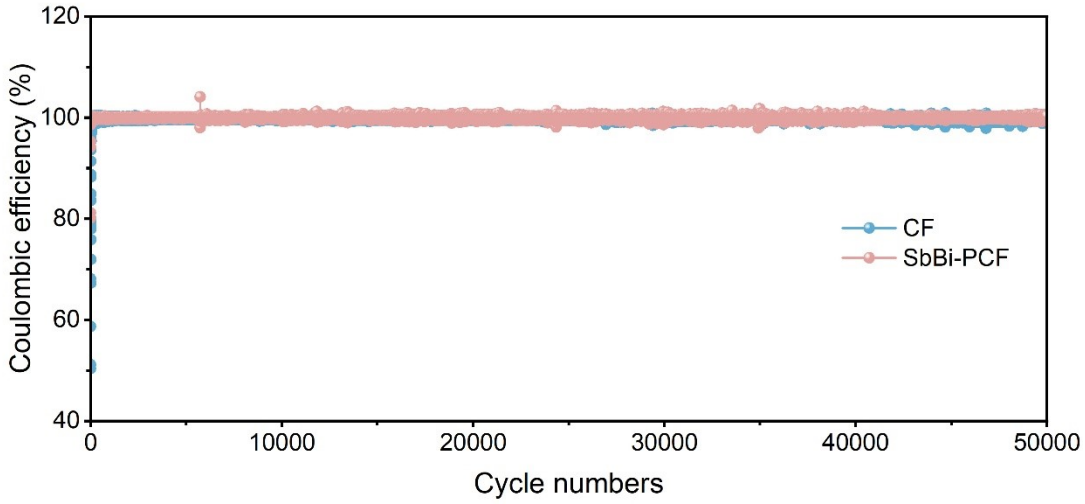

Fig. S6 Coulombic efficiency as a function of cycle numbers for CF and SbBi-PCF

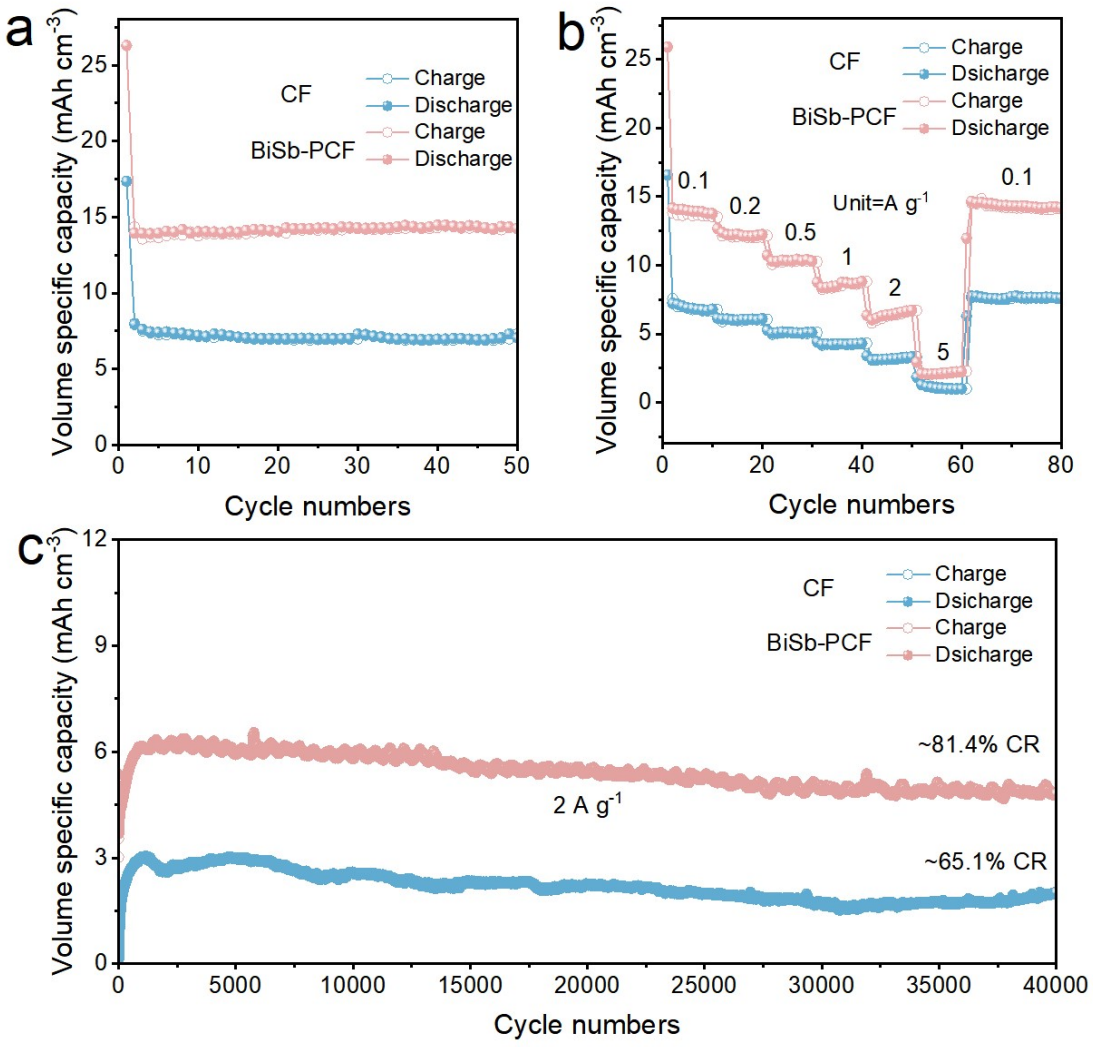

Fig. S7 Volume specific capacities. (a) Cycling performance, (d) Rate capability, and (e) Long cycling stability at high current of CF and SbBi-PCF.

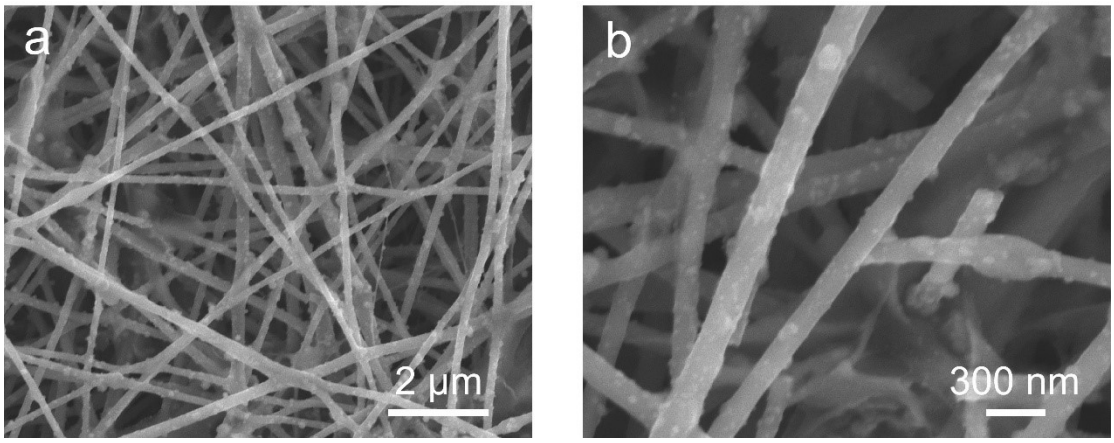

Fig. S8 Low- and high-magnification SEM images of the SbBi-PCF electrode after long-term cycling

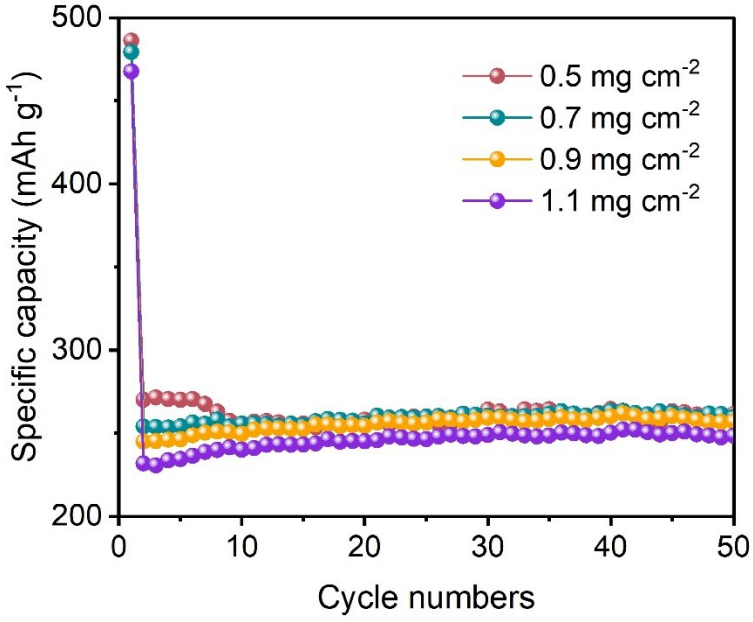

Fig. S9 Cycling stability of the SbBi-PCF electrode at a current density of 0.1 A g^{-1} with varying active material loadings (0.5-1.2 mg cm^{-2})

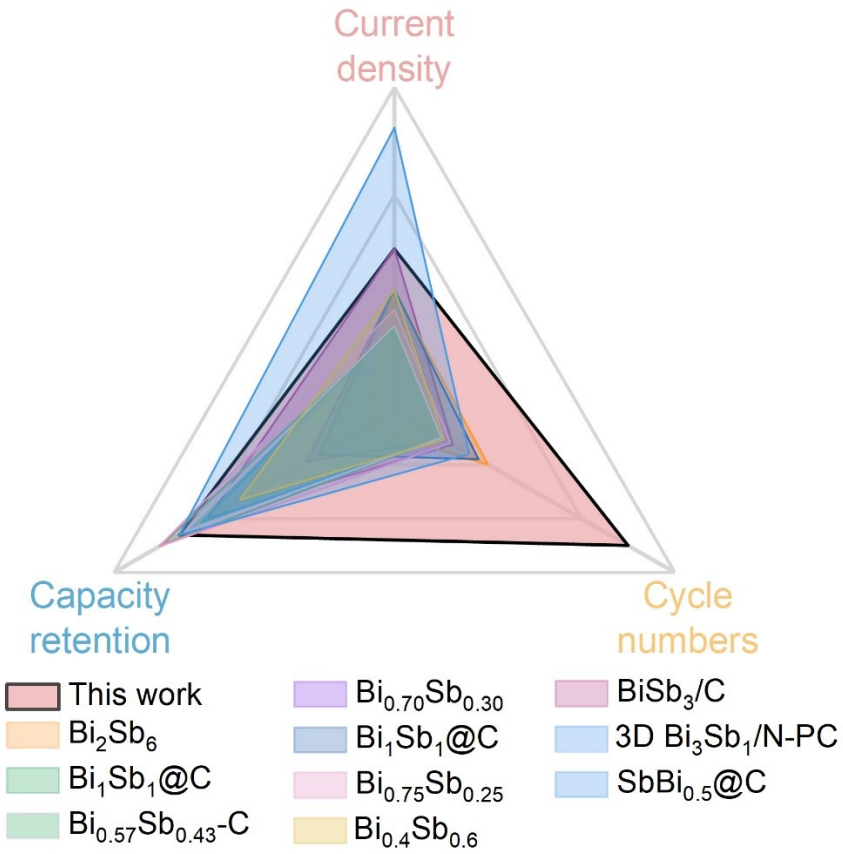

Fig. S10 Comparisons of current density, capacity retention and cycle performance between recently reported SbBi alloy-based anodes and this work.[1, 18-26]

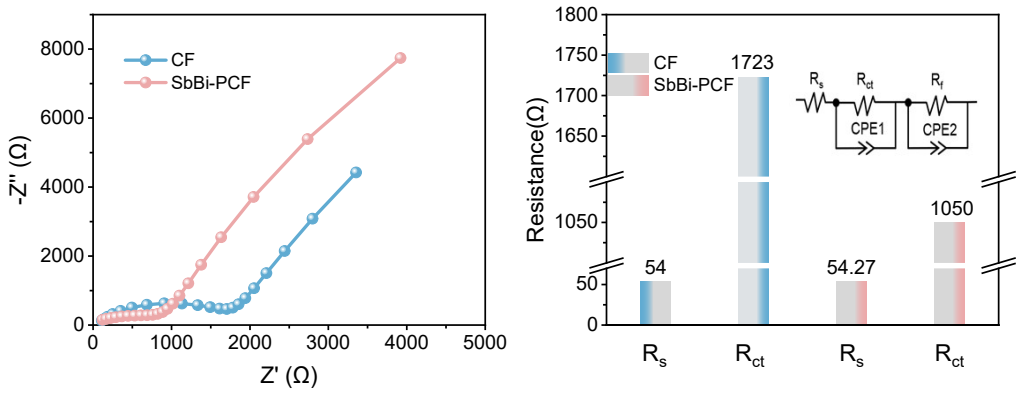

Fig. S11 (a)EIS spectra of CF and SbBi-PCF; (b) equivalent circuit and corresponding fitting results of CF and SbBi-PCF.

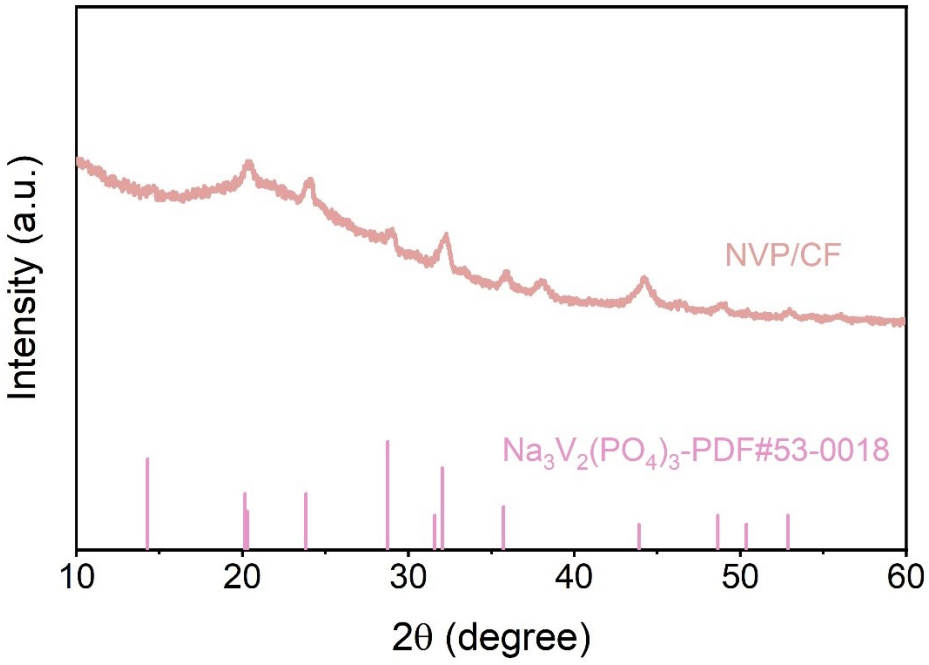

Fig. S12 XRD pattern of NVP/CF sample

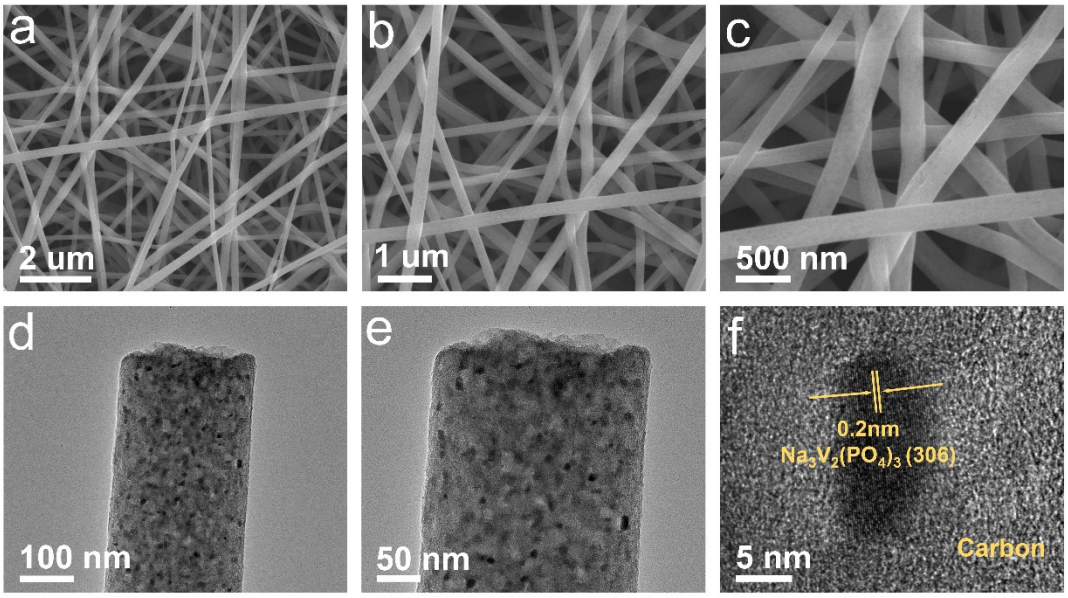

Fig. S13 (a-c) Low/high-magnification SEM images of NVP/CF sample; (d-f) Low/high-magnification TEM of NVP/CF sample

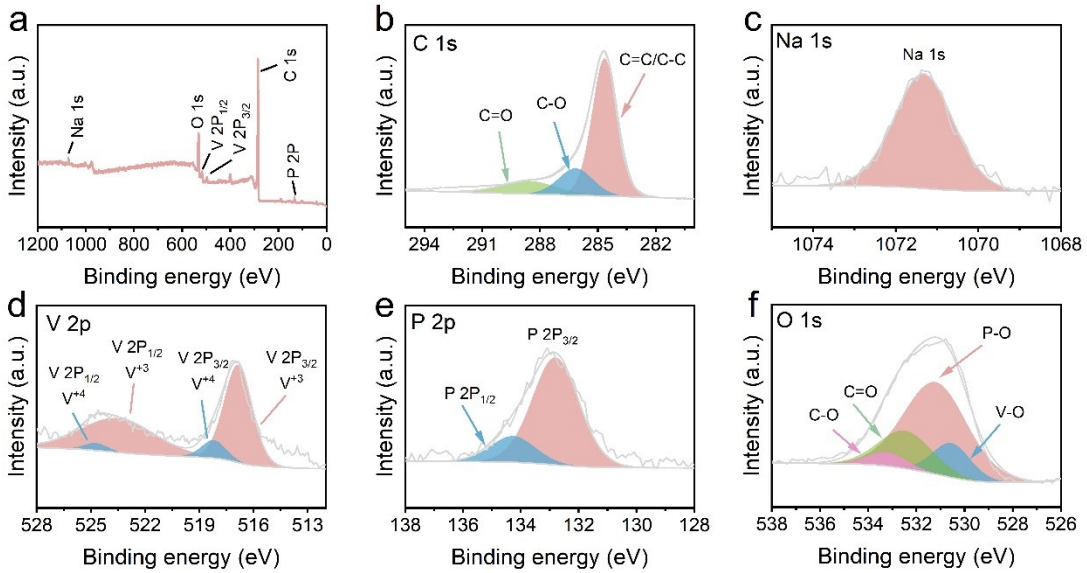

Fig. S14 (a) XPS full spectrum of NVP/CF sample; High-resolution XPS spectra of C 1s (b), Na 1s (c), V 2p (d), P 2p (e), and O 1s (f).

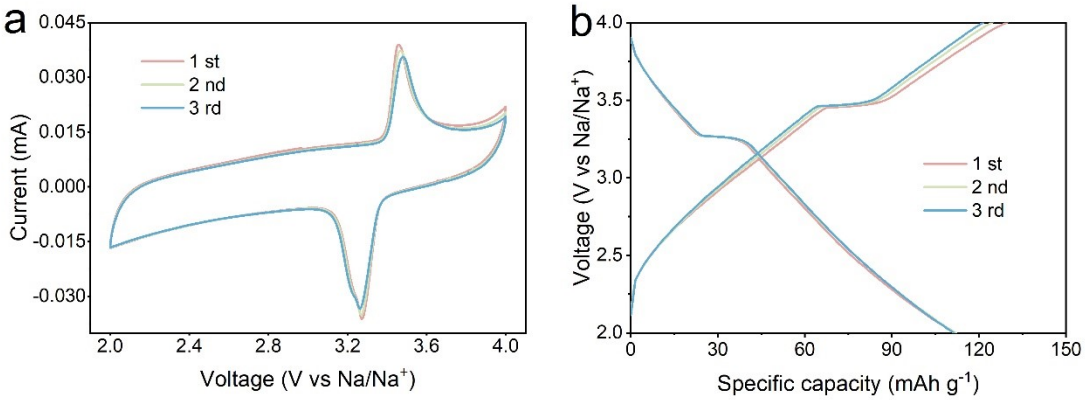

Fig. S15 Electrochemical performance of NVP/CF cathode (a) CV curves at 0.6 mV s^{-1}; (b) GCD profiles at 0.1 A g^{-1}.

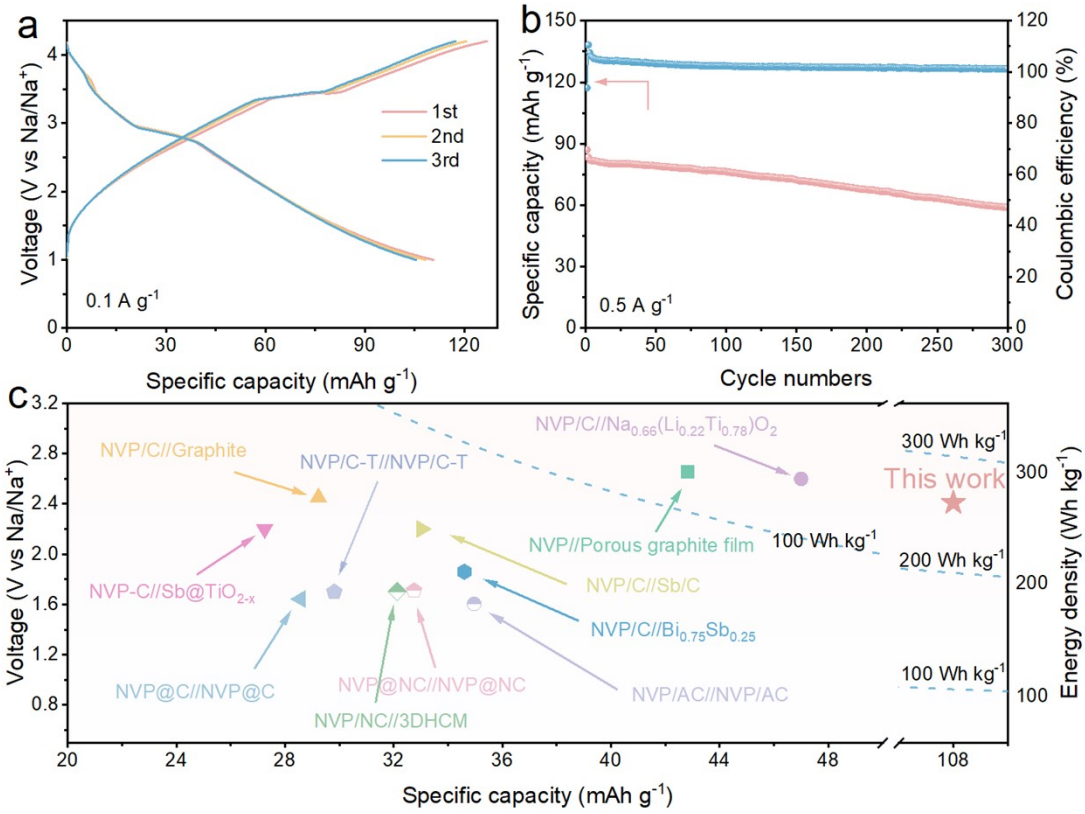

Fig. S16 Electrochemical performance of the SbBi-PCF//NVP/CF full cell: (a) GCD curves and (b) cycling performance of the SbBi-PCF//NVP/CF full cell; (c) Comparisons of specific capacity, energy density and voltage between related reported NVP-based SIBs.[1-11]

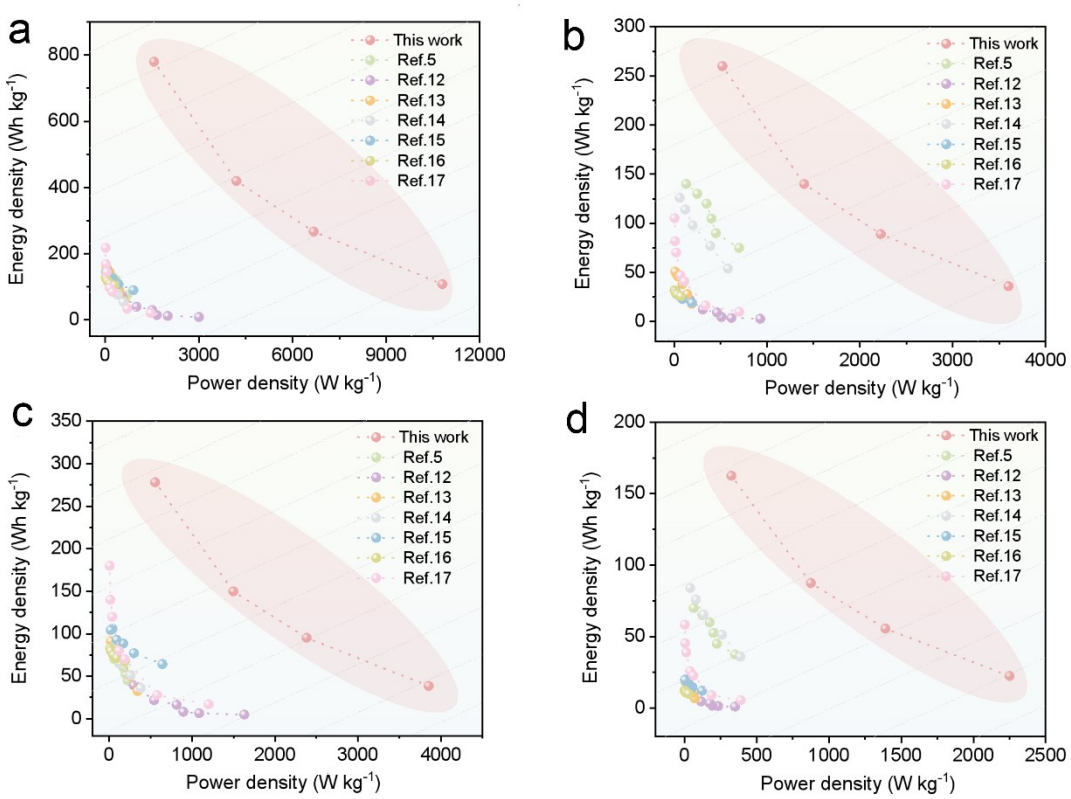

Figure S17 Comparison of energy density and power density between this work and recently reported Na-ion full cells (a) calculated based on the mass of cathode active material; (b) calculated based on cathode electrode mass; (c) calculated based on the total mass of both electrode active materials; (d) calculated based on complete device mass.[5,12-17]

Table S1. Comparisons of current density, capacity retention and cycle number between recently reported SbBi alloy-based anode and this work.[1, 18-26]

Anode	Cycle number	Current density (mA g^{-1})	Capacity retention (%)	Maximum specific capacity (mAh g^{-1} based on active material)
SbBi-PCF (This work)	50000	2000	73.5	877.7
$Bi_{0.70}Sb_{0.30}$	1000	1000	45.1	486.4
$BiSb_3$/C	2500	2000	73.1	561.0
Bi_2Sb_6	10000	1000	28.2	590.3
Bi_1Sb_1@C	8000	1000	41.6	476.2
3D Bi_3Sb_1/N-PC	6000	5000	81.4	391.2
Bi_1Sb_1@C	100	50	86.4	500.2
$Bi_{0.75}Sb_{0.25}$	2000	500	87.2	362.0
$SbBi_{0.5}$@C	100	100	75.3	396.0
$Bi_{0.57}Sb_{0.43}$-C	50	100	80.4	524.0
$Bi_{0.4}Sb_{0.6}$	700	64.1	1000	470.0

1. J. F. Ni, X. Y. Li, M. L. Sun, Y. F. Yuan, T. C. Liu, L. Li and J. Lu, *ACS Nano*, 2020, **14**, 9117.
2. J. X. Zhang, Y. J. Fang, L. F. Xiao, J. F. Qian, Y. L. Cao, X. P. Ai and H. X. Yang, *ACS Appl. Mater. Interfaces*, 2017, **9**, 7177.
3. W. Li, Z. J. Yao, C. A. Zhou, X. L. Wang, X. H. Xia, C. D. Cu and J. P. Tu, *Small*, 2019,

15, 1902432.

4. R. Ling, S. Cai, D. L. Xie, X. Li, M. J. Wang, Y. S. Lin, S. Jiang, K. E. Shen, K. Z. Xiong and X. H. Sun, *Chem. Eng. J.*, 2018, **353**, 264.
5. Y. S. Wang, X. Q. Yu, S. Y. Xu, J. M. Bai, R. J. Xiao, Y. S. Hu, H. Li, X. Q. Yang, L. Q. Chen and X. J. Huang, *Nat. Commun.*, 2013, **4**, 2858.
6. S. Li, Y. F. Dong, L. Xu, X. Xu, L. He and L. Q. Mai, *Adv. Mater.*, 2014, **26**, 3545.
7. W. C. Duan, Z. Q. Zhu, H. Li, Z. Hu, K. Zhang, F. Y. Cheng and J. Chen, *J. Mater. Chem. A*, 2014, **2**, 8668.
8. H. Wang, P. F. Hu, J. Yang, G. M. Gong, L. Guo and X. D. Chen, *Adv. Mater.*, 2015, **27**, 2348.
9. Z. Q. Yuan, L. L. Si and X. B. Zhu, *J. Mater. Chem. A*, 2015, **3**, 23403.
10. Z. Q. Zhu, F. Y. Cheng, Z. Hu, Z. Q. Niu and J. Chen, *J. Power Sources*, 2015, **293**, 626.
11. N. N. Wang, Z. C. Bai, Y. T. Qian and J. Yang, *Adv. Mater.*, 2016, **28**, 4126.
12. Y. Zhang, H. Y. Zhao, Y. P. Du, J. Mater. Chem. A 2016, **4**, 7155.
13. X. H. Yao, Z. X. Zhu, Q. Li, X. P. Wang, X. M. Xu, J. S. Meng, W. H. Ren, X. H. Zhang, Y. H. Huang, L. Q. Mai, ACS App. Mater. Interfaces 2018, **10**, 10022.
14. A. Das, S. B. Majumder, A. R. Chaudhuri, J. Power Sources 2020, **461**, 228149.
15. W. Wang, Q. J. Xu, H. M. Liu, Y. G. Wang, Y. Y. Xia, J. Mater. Chem. A 2017, **5**, 8440.
16. E. L. Gu, J. Y. Xu, Y. C. Du, X. F. Ge, X. S. Zhu, J. C. Bao, X. S. Zhou, J. Alloys Compd 2019, **788**, 240.
17. B. Pandit, M. T. Sougrati, B. Fraisse, L. Monconduit, Nano Energy 2022, **95**, 107010.
18. W. Zhang, W. Yan, H. Q. Jiang, C. Wang, Y. Zhou, F. H. Ke, H. J. Cong, H. X. Deng, , ACS Sustain. Chem. Eng. 2020, **8**, 335.
19. S. T. Guo, H. Li, Y. Lu, Z. F. Liu, X. L. Hu, Energy Storage Mater. 2020, **27**, 270.
20. H. Gao, J. Z. Niu, C. Zhang, Z. Q. Peng, Z. H. Zhang, ACS Nano 2018, **12**, 3568.
21. W. S. Ma, B. Yu, F. Q. Tan, H. Gao, Z. H. Zhang, Materials 2023, **16**.

22. X. X. Wang, B. Feng, L. M. Huang, Q. F. Fu, W. Z. Li, C. Zhu, P. Chen, C. L. Yang, Y. L. Ding, J Power Sources 2022, **520**, 230826.
23. J. J. Zhao, J. H. Xu, Q. Li, W. Yao, C. J. Yu, N. Zhang, X. J. Chen, X. L. Ding, Chem. 2023, **939**, 117452.
24. Q. X. Lin, J. Qin, Y. Y. Cao, X. K. Li, Y. Hong, M. C. Jin, J. J. Dong, W. Xiao, W. B. Li, J. J. Wang, X. F. Li, Chem. Eng. J. 2023, **474**, 145717.
25. Y. B. Zhao, A. Manthiram, Chem. Mater. 2015, **27**, 3096.
26. Y. Liu, X. Liu, X. Y. Wang, S. Ullah, Y. Peng, G. Y. Pan, W. J. Gao, B. Y. Song, X. H. Zhang, A. Jia, J. Wang, J. R. He, Y. P. Wu, Adv. Funct.Mater. 2025, **35**, 2415092.